Boletim da Sociedade Astronômica Brasileira, **36**, no. 1, 170-171
© SAB 2025

# Studying nonthermal radiation in stellar bowshock nebulae

D. P. Barbosa[1] & M. V. del Valle[1]

[1] Instituto de Astronomia, Geofísica e Ciências Atmosféricas da Universidade de São Paulo - IAG/USP
e-mail: deborapb@usp.br, mvdelvalle@usp.br

**Abstract.** Runaway stars are ejected from their formation sites and move at high velocities. In those systems, it is possible the formation of bowshock nebulae. It was confirmed that the radio emission observed in two of these bowshocks has a nonthermal origin. Therefore, in this work, we aim to determine whether other radio detections are of nonthermal origin and also to determine if they can emit gamma rays. Firstly, we compiled a small database containing physical parameters from bowshocks that have been detected at radio frequencies. Then, for all the sources, we estimated the relevant quantities for nonthermal emission production. We compared the kinetic power, acceleration time, and emissions for all the sources. We conclude that, at least, some of the analyzed stars can be nonthermal sources.

**Resumo.** Estrelas fugitivas são ejetadas de seus locais de formação e se movem em alta velocidade. Nesse tipo de sistema, é possível a formação de bowshocks estelares. Houve a confirmação de que a emissão em rádio observada em dois desses bowshocks é de origem não térmica. Sendo assim, neste trabalho queremos determinar se outras detecções em rádio também são de origem não térmica e também determinar se essas fontes podem ter emissão em raios gama. Primeiramente, reunimos uma pequena base de dados com parâmetros físicos de bowshocks que foram detectados em frequências de rádio. Então, para todas as fontes, estimamos as quantidades relavantes para produção de emissão não térmica. Comparamos gráficos da potência cinética, tempo de aceleração e emissões para todas as fontes. Concluimos que pelo menos algumas das canditadas são fontes de emissão não térmica.

**Keywords.** Acceleration of particles – Gamma rays: stars – Shock waves – Stars: winds, outflows

## 1. Introduction

Runaway stars have been expelled from their formation sites and move at high spatial velocities, V > 30 km/s (e.g., Hoogerwef et al. 2000; Tetzlaff et al. 2011). Among those stars, some are massive (> 10 $M_\odot$) and bright (> 3000 $L_\odot$), with spectral type O or B. It is possible to observe a bowshock nebula around them (e.g., van Buren et al. 1988), a phenomenon formed from the interaction of the stellar wind with the interstellar medium. These structures are observed in the infrared, produced by the dust present in the shocked medium.

Two of these bowshocks were detected in radio wavelengths and present nonthermal radiation emitted by highly energetic electrons via synchrotron mechanism (Benaglia et al. 2010; Moutzouri et al. 2022). This implies that the system can accelerate particles up to relativistic energies. Since these electrons can emit at high frequencies (del Valle & Romero 2012, 2014; del Valle & Pohl 2018), bowshocks from runaway stars become candidates for gamma-ray sources. However, it is not clear where the particles are accelerated. Furthermore, thermal emission in radio is also expected in these systems.

Studying the radio emission is thus critical as it often correlates with high-energy processes, such as particle acceleration, that also produce low-frequency radiation (e.g., Van del Eijden et al. 2022). By understanding these correlations, this work aims to make predictions about high-frequency radiation, specifically of gamma rays.

## 2. Bowshocks

A bowshock is a tridimensional structure similar to a spherical shell and optically thin. It is formed when a runaway star moves supersonically through the interstellar medium.

A steady state system of two shock waves separated by a discontinuity is developed. One shock is reverse, fast, adiabatic, and propagates in the stellar wind. The other is forward, slow, radiative, and propagates in the interstellar medium. The electrons responsible for the observed synchrotron emission can be accelerated in either shock.

Besides the dust emission, thermal Bremsstrahlung (free-free) is expected from the photoionized material. The high energy electrons can emit gamma rays, mainly through inverse Compton, synchrotron radiation, and relativistic Bremsstrahlung.

## 3. Data base

To analyze the desired sources (those that have radio emission), we created a small database containing the properties of the sources, Table 1. Next, we calculated the relevant quantities for the acceleration of particles and for the production of gamma rays, listed in Table 2.

## 4. Results

Figure 1 shows the kinetic power in the wind, $P_{\rm w}$, in the medium, $P_{\rm medium}$, and observed radio luminosity, $P_{\rm obs}$ ; Figure 2 compares the acceleration time in the medium, $t_{\rm acc(medium)}$, and in the wind, $t_{\rm acc(w)}$; Finally, Figure 3 compares the fluxes from free-free radiation, $S_{\rm ff}$, synchrotron radiation from the background electrons, $f_{\rm sync}$, and the observed, $S_{\rm obs}$.

Figure 1 suggests that, for HIP 88652 and HIP 98418, the significant difference between the observed and calculated power indicates that their luminosity may result from the interaction of accelerated particles in a shock. In contrast, for S1, K5, BD +43° 3654, and BD +60° 2522, the smaller difference between observed and calculated power suggests that the power of the resulting particles from the medium shock is too low to explain the observations. It is not possible to draw conclusions

**Table 1.** Data base with the properties of the analyzed stars.

| Name | G1 / NGC 6357 | G3 / NGC 6357 | S1 / RCW 49 | HIP 88652 | K5 / Cyg OB2 | HIP 98418 | HIP 38430 | BD+433654 | BD+60 2522 |
|---|---|---|---|---|---|---|---|---|---|
| **Spectral type** | O7.5-O7V | O6Vn-O5V | O5III | B0Ia | O9V | O7 | O6Vn+... | O4If | O6.5V |
| $T$ **(K)** | 35,500 | 39,870 | 40,310 | 20,000 | 33,400 | 30,000 | 38,870 | 40,700 | 36,200 |
| **Longitude** (°) | 353.42 | 353.30 | 284.08 | 151.19 | 79.82 | 71.58 | 243.16 | 82.41 | 112.23 |
| **Latitude** (°) | 0.45 | 0.08 | -0.43 | 3.33 | 0.10 | 2.87 | 0.36 | 2.33 | 0.22 |
| $S_\nu$ **($\mu$Jy)** | 8,000 | 5,970 | 12,600 | 2,240 | 11,150 | 5,300 | 31,700 | 155,556 | 822,222 |
| $\nu$ **(Hz)** | $8.88{\cdot}10^{8}$ | $8.88{\cdot}10^{8}$ | $8.88{\cdot}10^{8}$ | $8.88{\cdot}10^{8}$ | $8.88{\cdot}10^{8}$ | $8.88{\cdot}10^{8}$ | $8.88{\cdot}10^{8}$ | $4.50{\cdot}10^{9}$ | $4.50{\cdot}10^{9}$ |
| $S_\nu$**(erg s$^{-1}$ cm$^{-2}$)** | $7.10{\cdot}10^{-17}$ | $5.30{\cdot}10^{-17}$ | $1.12{\cdot}10^{-16}$ | $1.99{\cdot}10^{-17}$ | $9.90{\cdot}10^{-17}$ | $4.70{\cdot}10^{-17}$ | $2.81{\cdot}10^{-16}$ | $7.00{\cdot}10^{-15}$ | $3.70{\cdot}10^{-14}$ |
| $\dot{M}_w$ **(M$_\odot$ y r$^{-1}$)** | $2.00{\cdot}10^{-7}$ | $4.00{\cdot}10^{-7}$ | $3.23{\cdot}10^{-6}$ | $5.00{\cdot}10^{-8}$ | $5.00{\cdot}10^{-8}$ | $2.40{\cdot}10^{-7}$ | $7.00{\cdot}10^{-7}$ | $4.00{\cdot}10^{-6}$ | $1.30{\cdot}10^{-6}$ |
| $V_w$ **(km s$^{-1}$)** | 2.100 | 2.000 | 2.800 | 1.535 | 1.500 | 2.545 | 2.570 | 3.000 | 2.000 |
| $n_{ism}$ **(cm$^{-3}$)** | 14 | 16 | 30 | 2 | 2 | 380 | 60 | 6 | 27 |
| $D$ **(pc)** | 1,700 | 1,700 | 6,100 | 650 | 1,500 | 529.1 | 900 | 1,720 | 2,990 |
| $R_0$ **(pc)** | 0.4 | 0.49 | 1.24 | 0.28 | 0.44 | 0.08 | 0.13 | 1.48 | 0.37 |
| $V_{exp}$ **(km s$^{-1}$)** | 13.6 | - | - | 30 | 10 +/- 10 | 20 | 28 | 50 | 42 |
| $V_{calc}$ **(km s$^{-1}$)** | 24.30 | 25.61 | 24.85 | 39.27 | 24.70 | 28.13 | 74.76 | 53.63 | 47.07 |
| $Q_H$ **(s$^{-1}$)** | $4.07{\cdot}10^{48}$ | $1.26{\cdot}10^{49}$ | $3.02{\cdot}10^{49}$ | $4.30{\cdot}10^{47}$ | $1.78{\cdot}10^{49}$ | $1.00{\cdot}10^{49}$ | $9.77{\cdot}10^{48}$ | $1.66{\cdot}10^{49}$ | $1.35{\cdot}10^{49}$ |
| $a$ **(arcsec)** | 13.6 | 13.6 | 15.2 | 22.1 | 15.1 | 18.8 | 21.6 | 100 | 20 |
| $b$ **(arcsec)** | 12.8 | 12.8 | 13.1 | 15.9 | 13.8 | 12.9 | 15.6 | 50 | 20 |
| $c$ **(arcsec)** | 12.8 | 12.8 | 13.1 | 15.9 | 13.8 | 12.9 | 15.6 | 50 | 20 |

**Table 2.** Data base with the calculated properties of the analyzed stars.

| Name | G1 / NGC 6357 | G3 / NGC 6357 | S1 / RCW 49 | HIP 88652 | K5 / Cyg OB2 | HIP 98418 | HIP 38430 | BD+433654 | BD+60 2522 |
|---|---|---|---|---|---|---|---|---|---|
| $P_w$ **(erg s$^{-1}$)** | $2.78{\cdot}10^{33}$ | $5.05{\cdot}10^{33}$ | $7.98{\cdot}10^{34}$ | $3.71{\cdot}10^{32}$ | $3.55{\cdot}10^{32}$ | $4.90{\cdot}10^{33}$ | $1.46{\cdot}10^{34}$ | $1.14{\cdot}10^{35}$ | $1.64{\cdot}10^{34}$ |
| $P_{medium}$ **(erg s$^{-1}$)** | $3.22{\cdot}10^{31}$ | $6.46{\cdot}10^{31}$ | $7.09{\cdot}10^{32}$ | $9.50{\cdot}10^{30}$ | $5.84{\cdot}10^{30}$ | $5.42{\cdot}10^{31}$ | $4.24{\cdot}10^{32}$ | $2.03{\cdot}10^{33}$ | $3.86{\cdot}10^{32}$ |
| $P_{obs}$ **(erg s$^{-1}$)** | $2.46{\cdot}10^{28}$ | $1.83{\cdot}10^{28}$ | $4.98{\cdot}10^{29}$ | $1.01{\cdot}10^{27}$ | $2.66{\cdot}10^{28}$ | $1.58{\cdot}10^{27}$ | $2.73{\cdot}10^{28}$ | $2.48{\cdot}10^{30}$ | $3.96{\cdot}10^{31}$ |
| $R_S$ **(pc)** | 8.26 | 11.00 | 9.69 | 14.28 | 49.38 | 1.23 | 4.19 | 23.20 | 7.94 |
| $B_{medium}$ **(gauss)** | $3.74{\cdot}10^{-6}$ | $4.00{\cdot}10^{-6}$ | $5.48{\cdot}10^{-6}$ | $1.41{\cdot}10^{-6}$ | $1.41{\cdot}10^{-6}$ | $1.95{\cdot}10^{-5}$ | $7.75{\cdot}10^{-6}$ | $2.45{\cdot}10^{-6}$ | $5.20{\cdot}10^{-6}$ |
| $B_w$ **(gauss)** | $1.32{\cdot}10^{-6}$ | $1.49{\cdot}10^{-6}$ | $1.97{\cdot}10^{-6}$ | $8.05{\cdot}10^{-7}$ | $5.06{\cdot}10^{-7}$ | $7.95{\cdot}10^{-6}$ | $8.40{\cdot}10^{-6}$ | $1.90{\cdot}10^{-6}$ | $3.55{\cdot}10^{-6}$ |
| $E_{medium}$ **(GeV)** | 3.85 | 3.72 | 3.18 | 6.26 | 6.26 | 1.69 | 2.67 | 10.71 | 7.35 |
| $E_w$ **(GeV)** | 6.48 | 6.11 | 5.30 | 8.29 | 10.50 | 2.64 | 2.57 | 12.10 | 8.90 |
| $t_{acc(medium)}$ **(s)** | $6.75{\cdot}10^{-14}$ | $6.78{\cdot}10^{-14}$ | $3.98{\cdot}10^{-14}$ | $7.58{\cdot}10^{-13}$ | $3.00{\cdot}10^{-13}$ | $7.60{\cdot}10^{-15}$ | $2.14{\cdot}10^{-13}$ | $1.40{\cdot}10^{-12}$ | $3.48{\cdot}10^{-13}$ |
| $t_{acc(w)}$ **(s)** | $2.41{\cdot}10^{-9}$ | $1.83{\cdot}10^{-9}$ | $2.34{\cdot}10^{-9}$ | $2.70{\cdot}10^{-9}$ | $5.16{\cdot}10^{-9}$ | $2.39{\cdot}10^{-10}$ | $2.25{\cdot}10^{-10}$ | $6.38{\cdot}10^{-9}$ | $1.12{\cdot}10^{-9}$ |
| $S$ | 22.85 | 24.08 | 23.36 | 36.91 | 23.22 | 26.44 | 70.28 | 50.42 | 44.25 |
| $\epsilon_{ff}$ **(erg s$^{-1}$ cm$^{-3}$ Hz$^{-1}$)** | $1.33{\cdot}10^{-36}$ | $1.74{\cdot}10^{-36}$ | $6.12{\cdot}10^{-36}$ | $2.72{\cdot}10^{-38}$ | $2.72{\cdot}10^{-38}$ | $9.82{\cdot}10^{-34}$ | $2.45{\cdot}10^{-35}$ | $2.45{\cdot}10^{-37}$ | $4.96{\cdot}10^{-36}$ |
| $V$ **(cm$^3$)** | $1.54{\cdot}10^{53}$ | $1.54{\cdot}10^{53}$ | $8.31{\cdot}10^{54}$ | $2.15{\cdot}10^{52}$ | $1.36{\cdot}10^{53}$ | $6.50{\cdot}10^{51}$ | $5.38{\cdot}10^{52}$ | $1.78{\cdot}10^{55}$ | $3.00{\cdot}10^{54}$ |
| $S_{ff}$**(erg s$^{-1}$ cm$^{-2}$)** | $5.25{\cdot}10^{-19}$ | $6.86{\cdot}10^{-19}$ | $1.01{\cdot}10^{-17}$ | $1.03{\cdot}10^{-20}$ | $1.22{\cdot}10^{-20}$ | $1.69{\cdot}10^{-16}$ | $1.20{\cdot}10^{-17}$ | $5.55{\cdot}10^{-17}$ | $6.25{\cdot}10^{-17}$ |
| $L_{sinc}$**(erg s$^{-1}$)** | $2.84{\cdot}10^{23}$ | $3.33{\cdot}10^{23}$ | $3.19{\cdot}10^{25}$ | $8.79{\cdot}10^{21}$ | $4.08{\cdot}10^{22}$ | $2.93{\cdot}10^{23}$ | $8.23{\cdot}10^{23}$ | $3.10{\cdot}10^{25}$ | $1.96{\cdot}10^{25}$ |
| $f_{sinc}$**(erg s$^{-1}$ cm$^{-2}$)** | $8.20{\cdot}10^{-22}$ | $9.64{\cdot}10^{-22}$ | $7.16{\cdot}10^{-21}$ | $1.74{\cdot}10^{-22}$ | $1.52{\cdot}10^{-22}$ | $8.74{\cdot}10^{-21}$ | $8.50{\cdot}10^{-21}$ | $8.75{\cdot}10^{-20}$ | $1.83{\cdot}10^{-20}$ |

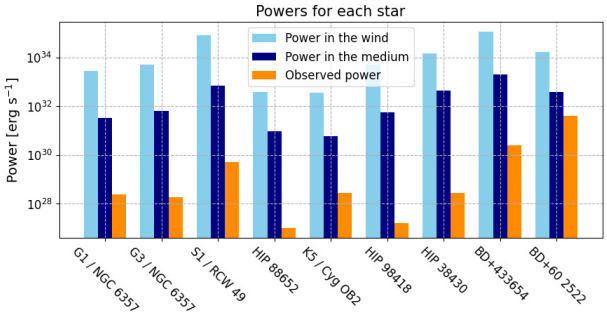


**Figure 1.** Comparison of different powers for each star.

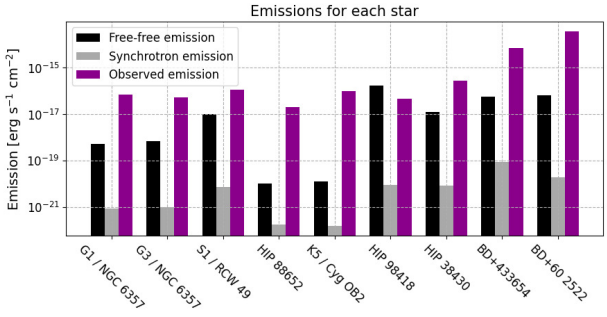


**Figure 3.** Comparison of different emissions for each star.

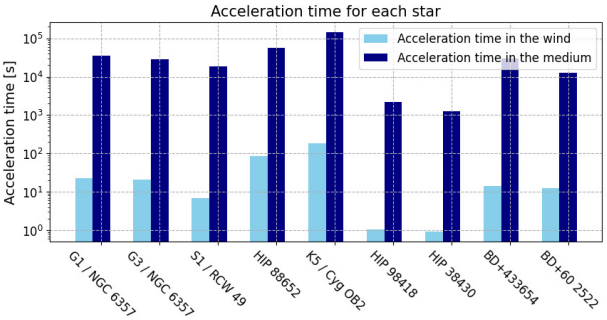


**Figure 2.** Comparison of acceleration times for each star.

from the intermediate cases. However, from Figure 2, we can conclude that the particle acceleration is more likely to happen in the wind.

Besides that, according to Figure 3, for HIP 88652 and K5 stars, it is likely that the observed radiation is produced by synchrotron radiation from locally accelerated electrons because the free-free emission is too low to explain it. For HIP 98418, we can see that some of its parameters were overestimated since our free-free radiation estimation can not be greater than the observed emission.

Finally, since G1, G3, BD +43° 3654, and BD +60° 2522 have free-free radiation far below the observed emission, but not as low as HIP 88652 and K5, we can conclude that there is a possibility that the synchrotron radiation component is larger than the thermal one.

The contribution from cosmic ray electrons is negligible in all cases (see Figure 3), so we can affirm there is the possibility that at least some of the analyzed stars possess a strong nonthermal component, produced by electrons accelerated locally. As the next step, we will apply a radiative model to all the stars.

*Acknowledgements.* This work is supported by FAPESP project 2019/05757-9. D.P.B. is supported by 'Programa Institucional de Bolsas de Iniciação Científica' (Process 2023-2254).

## References

Benaglia, P., Romero, G. E., Mart J., Peri, C. S., & Araudo, A. T. 2010, A&A, 517, L10
del Valle, M. V., & Romero, G. E. 2012, A&A, 543, A56
del Valle, M. V., & Romero, G. E. 2014, A&A, 563, A96
del Valle, M. V. & Pohl M. 2018, ApJ, 864, 19
Hoogerwerf, R., de Bruijne, J. H. J., & de Zeeuw, P. T. 2000, ApJL, 544, L133
Moutzouri, M., Mackey, J., Carrasco-Gonzalez, C., et al. 2022, A&A, 663, A80
Tetzlaff , N., Neuhuser, R., & Hohle, M. M. 2011, MNRAS, 410, 190
van Buren, D., & McCray, R. 1988, ApJL, 329, L93
Van den Eijnden, J. and Saikia, P. and Mohamed, S., 2022, MNRAS, 512, 5374